**RESEARCH ARTICLE**

WILEY *polymers advanced technologies*

# Poly(p-phenylenediamine)-coated magnetic particles: Preparation and electrochemical properties

Ernandes Taveira Tenório-Neto[1,2] | Abdoullatif Baraket[3] |
Marcos Rogério Guilherme[4] | Michele Karoline Lima-Tenório[1,2] | Quentin Lelong[1] |
Nadia Zine[3] | Abdelhamid Errachid[3] | Hatem Fessi[1] | Abdelhamid Elaissari[1]

[1] Univ Lyon, University Claude Bernard Lyon-1, CNRS, LAGEP-UMR 5007, Lyon F-69622, France

[2] Department of Chemistry, State University of Ponta Grossa, Ponta Grossa, Paraná, Brazil

[3] Institute of Analytical Sciences, UMR 5280, Claude Bernard Lyon 1 University, University of Lyon, Villeurbanne, France

[4] Department of Chemistry, State University of Maringá, Maringá, Paraná, Brazil

**Correspondence**
Abdelhamid Elaissari, Univ Lyon, University Claude Bernard Lyon-1, CNRS, LAGEP-UMR 5007, F-69622 Lyon, France.
Email: abdelhamid.elaissari@univ-lyon1.fr

**Funding information**
Campus France, Grant/Award Number: PHC PROCOPE 40544QH; Science Without Borders program, Grant/Award Numbers: 249058/2013-8 and 249056/2013-5; KardiaTool European Project, Grant/Award Number: 768686; European Union's Horizon 2020 Research and Innovation Programme, Grant/Award Number: 643694

Magnetic particles are of great interest in various biomedical applications, such as, sample preparation, in vitro biomedical diagnosis, and therapy. For biosensing applications, the used functional magnetic particles should answer numerous criteria such as; submicron size in order to avoid rapid sedimentation, high magnetic content for fast separations under applied magnetic field, and finally, good colloidal stability. Therefore, the aim of this work was to prepare submicron magnetic core and conducting polymer shell particles. The polymer shell was induced using p-phenylenediamine as key monomer. The obtained core–shell particles were characterized in terms of particle size, size distribution, magnetization properties, Fourier transform infrared (FTIR) analysis, surface morphology, chemical composition, cyclic voltammetry, and impedance spectroscopy. The best experimental condition was found using 40 mg of povidone (PVP—stabilizing agent) and 0.16 mmol of p-phenylenediamine. Using such initial composition, the core-shell magnetic nanoparticles shown a narrowed size distribution around 290 nm and high magnetic content (above 50%). The obtained amino containing submicron highly magnetic particles were found to be a conducting material and superparamagnetic in nature. These promising conducting magnetic particles can be used for both transport and *lab-on-a-chip* detection.

**KEYWORDS**

seeded polymerization, conducting polymer, cyclic voltammetry, sensor, magnetic emulsion

## 1 | INTRODUCTION

Magnetic nanocomposites have attracted much attention because of their promising properties, which can be used in diverse technologies, including, microsystems, *lab-on-chip*, biosensing applications, purification, cancer therapy, nucleic acid extraction and purification, and specific capture of analyte in biological samples etc.[1-3] When applied in biosensing, these nanocomposites act as concentrator providing good detection sensitivity of the target. In this sense, using superparamagnetic nanoparticles (MNPs) offer a great advantage over normal polymer or silica particles. When superparamagnetic particles are used, the particles are found to be easy to disperse after applying external magnetic field and no aggregation phenomena have been observed.[4] Among magnetic nanoparticles, iron oxides and in particular magnetite ($Fe_3O_4$) and its oxidized form maghemite ($\gamma$-$Fe_2O_3$), have attracted much attention because of their high specific magnetization property, biocompatibility, low toxicity, and easy to preparation at low cost.[5,6]

Obtaining superparamagnetic hybrid materials with desired properties, and also with specific functional groups, have been reported

by several authors using various approaches.[7-11] These approaches can be divided into (a) physical-based process (e.g., sequential adsorption of oppositely charged polyelectrolytes) and (b) chemical encapsulation via polymerization in disperse media (e.g., surface functionalization/modification of MNPs via specific grafting, surface initiated controlled polymerization, inorganic silica/polymer hybridization, or by heterogeneous polymerization in dispersion media).[9]

For biosensing applications, the MNPs have been combined with conducting polymers to provide a new class of material with both magnetic and electric properties.[7,12] Conducting polymers (CPs) are carbon-based molecules, which exhibit electrical, optical, and electronic properties analogous to metals. However, CPs have some advantages compared with metals, such as, flexibility, low toxicity, easy processing, and especially, low cost. All these characteristics make CPs potential materials for applications in sensors, fuel cells, energy storage, and so forth.[3,10] In sensors field, the charge transport properties of conducting polymers are changed when exposed to targeted analytes. The captured analyte amount can be directly correlated to the measured signal. Polyaniline (PANI), polypyrrole (PPy), polythiophene, poly(p-phenylenediamine) (PPDA), and their derivatives are a class of CPs which are most studied because of their facile synthesis and flexibility in processing.[13] Among the CPs, the poly (phenylenediamines) have attracted more attention, especially in the biomedical field, where the potential toxicity of aniline and its oligomers is feared.[14]

In the literature, there are several studies combining magnetic nanoparticles and PPDA using emulsion polymerization technique.[15,16] However, the reported researches consist of producing only magnetic nanocomposites. In order to take advantage of conductive properties of PPDA and to improve the accuracy of the biosensing event, we investigated the synthesis route, as well as, the key parameters leading to hybrid submicron core-shell particles containing MNPs-core and PDA-shell. The core-shell morphology offers new possibilities for new applications. For example, because of its polymeric core, the surface can be easily modified to interact with a desired analyte, enhancing the signal detection and transmission (for biosensor) or even providing fast separations of the analyte by an external magnetic field. Moreover, the core-shell nanoparticles may be used as template for producing new morphologies such as hollow particles.

To prepare core-shell nanoparticles, the magnetic emulsion (ME), containing superparamagnetic iron oxide nanoparticles, was used as seed in a seeded-emulsion polymerization approach. Then, the polymerization of p-phenylenediamine (PDA) was carried out to obtain $NH_2$-functionalized CPs on the particle surface. The influence of both the amount of the monomer and the stabilizing agent on the final morphology of the nanoparticles were evaluated. The obtained magneto-conductingcore/shell nanoparticles were characterized in terms of chemical composition, particle size and size distribution, morphology, and magnetic behavior. Then, electrodeposition assays, cyclic voltammetry, and impedance spectroscopy were performed to ascertain the potential of magneto-conductingcore/shell nanoparticles in biosensor applications.

## 2 | EXPERIMENTAL

### 2.1 | Materials

Potassium persulfate 99+% (KPS) and PVP were purchased from Sigma-Aldrich. Oil in water ME (total solid content 7.9%, average size distribution 193 ± 5 nm) consisting of superparamagnetic nanoparticles stabilized with oleic acid, octane, and dodecyl sodium sulfate was from Ademtech S. A (Bordeaux, France). PDA, 99+%, was purchased from Acros Organics. All reagents were used without further purification and aqueous solutions were prepared with deionized water.

### 2.2 | Synthesis of PPDA-coated magnetic particles

The seeded-emulsion polymerization was performed upon addition of 1.52 g of ME (0.12 g dried extract) into a 25-mL glass reactor being mechanically stirred with a Teflon paddle. Then, the supernatant was removed from the mixture after 3 minutes of magnetic separation. After that, 7.5 mL of a solution containing known amounts of PVP (as stabilizing agent) and PDA (as monomer) were brought into the reactor. The solution was kept at 300 rpm for 4 hours. Later, 7.5 mL of an acidic solution (HCl 0.1 mol $L^{-1}$) containing 43.2 mg (0.16 mmol) of KPS was added dropwise (0.5 mL $min^{-1}$), while stirring (see samples composition in Table 1). The mixture was left to react for 20 hours under stirring at room temperature.

Herein, the samples were labeled according to their initial composition: The amounts of PVP (in mg) are indicated at the first two digits, while the amount of PDA (in mmol) is indicated at last ones. For example, sample 2032 means 20 mg of PVP and 0.32 mmol of PDA used in the seeded polymerization. All other reactants concentrations were kept constant.

## 3 | CHARACTERIZATION

### 3.1 | Transmission electron microscopy

Transmission electron microscopy (TEM) images were obtained with a Philips CM120 microscope at the "Centre Technologique des Microstructures" at the University of Lyon (Villeurbanne, France). A small drop of suspension was deposited on a microscope grid (copper support covered with carbon) and slowly dried in open air. The dried samples were observed by bright field TEM applying 120 kV acceleration voltage.

### 3.2 | Particle size and zeta potential measurements

A Malvern Zetasizer (Nano ZS, Malvern Instruments Limited, UK) was used to measure both the particle size, size distribution, and the zeta potential of the magnetic polymer colloidal particles. The magnetic samples were dispersed in a $10^{-3}$ mol $L^{-1}$ NaCl solution. Then, the

**TABLE 1** Compositions of stabilizer (PVP) and monomer (PDA) used in the seeded polymerization[a]

| Sample Name | PVP, mg | PDA, mmol |
| --- | --- | --- |
| 0000[b] | 0.0 | 0.00 |
| 0008 | 0.0 | 0.08 |
| 0016 | 0.0 | 0.16 |
| 0032 | 0.0 | 0.32 |
| 1000 | 10.0 | 0.00 |
| 1008 | 10.0 | 0.08 |
| 1016 | 10.0 | 0.16 |
| 1032 | 10.0 | 0.32 |
| 2000 | 20.0 | 0.00 |
| 2008 | 20.0 | 0.08 |
| 2016 | 20.0 | 0.16 |
| 2032 | 20.0 | 0.32 |
| 4000 | 40.0 | 0.00 |
| 4008 | 40.0 | 0.08 |
| 4016 | 40.0 | 0.16 |
| 4032 | 40.0 | 0.32 |

Abbreviations: PDA, *p*-phenylenediamine; PVP, povidone.

[a]0.16 mmol of KPS was used in the seeded polymerization at RT for 20 hours.

[b]Reference Sample.

particle size distribution was obtained taking into consideration the average of at least five measurements (10 runs for each colloidal dispersion).

The zeta potential was obtained as function of pH at 25°C. The measurements were performed using a highly diluted dispersion of the colloidal particles in a $10^{-3}$ mol $L^{-1}$ NaCl solution. The pH was adjusted using solutions of 0.1 mol $L^{-1}$ NaOH or 0.1 mol $L^{-1}$ HCl. The recorded value was considered as the average of three measurements.

## 3.3 | Fourier transformed infrared

The surface properties of the samples were investigated using an attenuated total reflexion-Fourier transformed infrared spectrophotometer (ATR-FTIR), Shimadzu, Japan. All samples were wiped off and dried before analysis. The spectra were scanned over a range of 4000 to 400 $cm^{-1}$.

## 3.4 | Thermogravimetric analysis

Thermogravimetric (TG) analysis measurements were carried out on a TG analyzer (NETZSCH-TG209F1 Iris®ASC). The measurements were performed under an $N_2$ atmosphere (50 mL $min^{-1}$), starting from room temperature up to 1000°C, at a heating rate of 10°C $min^{-1}$. Before analysis, the samples were separated from the supernatant by applying permanent magnetic field and then washed with deionized water

to remove the nonmagnetic materials, such as surfactant and free polymer particles. After that, the samples were left to dry at 40°C for 24 hours before TG analysis.

## 3.5 | Cyclic voltammetry and electrochemical impedance spectroscopy measurements

Electrochemical characterizations were carried out by using a VMP-3 potentiostat (Biologic CE-Lab VMP3). All measurements for cyclic voltammetry (CV) and electrochemical impedance spectroscopy (EIS) measurements were made at room temperature (approximately 24°C). The electrolyte for both CV and EIS measurements was made from a redox probe using ferro- and ferricyanide $K_3(Fe (CN)_6)/K_4(Fe (CN)_6)$ at $5 \times 10^{-3}$ mol $L^{-1}$ in PBS buffer (pH 7.4). Electrochemical measurements were made within a Teflon cell in which the gold working electrode (WE) was sandwiched between the two parts of the electrochemical cell (see Figure S2). Platinum wire was used as the counter electrode (CE) and a calomel saturated electrode was used as the reference electrode (RE). The gold area exposed to the electrolyte was approximately 3 mm in diameter. The volume of ferrocyanide buffer was affixed for all measurements at 1.3 mL.

## 3.6 | Magnetic properties

Magnetization measurements were carried out using the Automatic Bench of Magnetic Measurements (ABMM) at CNRS-IRC Lyon laboratory, France. Samples were dried and magnetization was investigated at room temperature by varying the magnetic field (H) from −20000 to +20000 Oe.

## 4 | RESULTS

### 4.1 | Investigating the experimental parameters for preparing core-shell particles

Excellent colloidal dispersion of magnetic particles can be achieved when there is a balance between the attractive and the repulsive forces. In case of magnetic emulsions, the repulsive forces are dominating mainly because of their negatively charged surface.[17] However, the intensity of the repulsive forces may be decreased upon addition of an acidic solution. In such a condition, the attractive forces (because of the magnetic interaction) are formed in the emulsion, leading the small particles to coalesce into larger ones.

For preparing core-shell nanoparticles, using PPDA, an acidic environment is required for solubilizing the PDA monomers (see Section 2.2). Thus, to avoid the coalescence of the nanoparticles during the experiments, PVP was used as stabilizing agent. We hypothesized that the PVP could act as a steric barrier between the magnetic particles, preventing their coalescence [7,18]. Therefore, the influence of PVP amount on stabilizing the magnetic emulsion was investigated. The samples evaluated were: 0000, 1000, 2000, and 4000 (0 mg, 10 mg,

20 mg, and 40 mg of PVP, respectively) and the results are shown in Figure 1 (A-D).
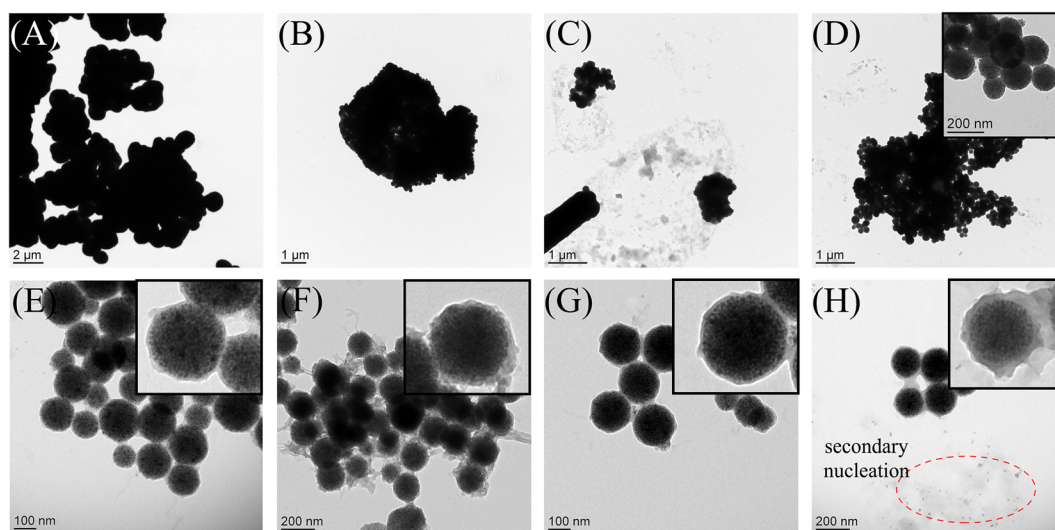
The magnetic emulsion (sample 0000), Figure 1A, was immediately precipitated after addition of acid solution (see Figure S1). As explained earlier, this effect is the result of a decrease in negative surface charges on the magnetic particles, because of increased acidity of the magnetic emulsion. At this condition, the attractive forces became more important (by magnetic attraction), leading to coalescence of the particles. In fact, the ME could be stabilized, in acid environment, only when the amount of PVP was higher than 20 mg (Figure 1C,D).

In a second test, the influence of PDA in the emulsion stabilization was also investigated. Polymerization reactions containing 0.08, 0.16, and 0.32 mmol of PDA were performed without PVP (samples 0008, 0016, and 0032, respectively). However, regardless of the concentration, the PDA did not show any significant effect on stabilizing the emulsion. In addition, in such experimental condition, we observed phase separation, where the PPDA was polymerized without magnetic core and the magnetic particles remained agglomerated (data not shown).

In fact, core-shell morphology was only observed when the amount of PVP and PDA were, respectively, higher than 20 mg and 0.16 mmol (samples 2016, 2032, 4016, and 4032). TEM images of the core-shell nanoparticles are shown in Figure 1E-H.

For sample 2016 (Figure 1E), a core-shell morphology, with a thin layer of PPDA, was observed. If compared with sample 4016 (Figure 1G), the final morphology was shown to be almost the same. This result suggests that PVP did not play any influence on the final morphology, being only necessary for stabilizing the ME. However, when the amount of PDA was increased from 0.16 mmol (sample 2016, Figure 1E) to 0.32 mmol (sample 2032, Figure 1F), the polymeric layer became thick and rough. Moreover, polymeric particles, without magnetic core, were observed. The formation of such particles has been thought to be the result of secondary nucleation (Figure 2).[17]

During the initial stage of emulsion polymerization, the oligomeric radicals of PDA diffuse into the oil droplets leading to the formation of core-shell nanoparticles. However, when the concentration of monomer is high, the oligomers may undergo homogeneous nucleation generating polymeric particles without magnetic core.[19,20] This effect is better observed in the samples 2032 and 4032, both with the highest



**FIGURE 1** (A-D) Bright field transmission electron microscopy (TEM) images of magnetic emulsion (ME) after the acidification step: (A) 0000, (B) 1000, (C) 2000, and (D) 4000. (E-H) TEM images of samples obtained after polymerization of *p*-phenylenediamine (PDA) using ME as seed: (E) 2016, (F) 2032, (G) 4016, and (H) 4032 [Colour figure can be viewed at wileyonlinelibrary.com]
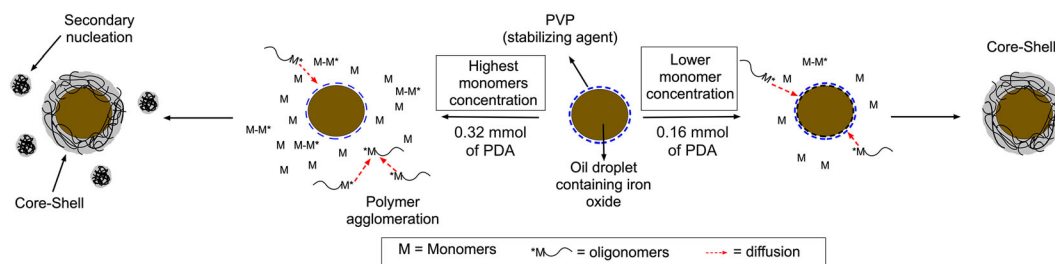


**FIGURE 2** Scheme suggesting the different ways for producing core-shell nanoparticles by seeded-emulsion polymerization [Colour figure can be viewed at wileyonlinelibrary.com]

concentration of PDA (0.32 mmol, Figure 1F,H). On the basis of the observations described above, the samples 2016 and 4016 were chosen as those from the best experimental condition in the production of core-shell type particles.

## 4.2 | Fourier transformed infrared

Figure 3A shows the FTIR spectra of ME, sample 2016, and sample 4016 in the spectral range of 2000 $cm^{-1}$ to 400 $cm^{-1}$. ME was obtained after the emulsification of ferrofluid (oil phase) in aqueous solution with surfactant. Moreover, in the oil phase, the iron oxide particles were stabilized with oleic acid (OA).

In the ME spectra, an absorption band appeared at approximately 1700 $cm^{-1}$, because of C=O stretching vibration of free OA. In addition, a high-intensity band at approximately 570 $cm^{-1}$ (ascribed to Fe—O stretching vibration), which was observed in all the spectra, is associated to the magnetic phase in the polymer particles.[7]

The samples 2016 and 4016 showed same spectral profile, which is more likely to be from the same polymer shell. The absorption bands at 1650 $cm^{-1}$ and 1510 $cm^{-1}$ are associated, respectively, with C—H stretching from quinonoid and benzenoid rings,[21] while the band, at 1580 $cm^{-1}$, was attributed to C=N stretching.[22] In addition, the bands at 1270 $cm^{-1}$ and 1160 $cm^{-1}$ were attributed to C—N stretching from benzenoid and quinonoid rings and the band at 1508 $cm^{-1}$ is the result from C=C stretching.[21]

## 4.3 | Magnetic properties

Magnetic curves for the dried latexes obtained by seeded polymerization are presented in Figure 3B. According to the papers published elsewhere, saturation magnetization ($M_S$) of iron oxide can be found between 60 emu $g^{-1}$ and 80 emu $g^{-1}$ depending on the predominant crystalline phase.[23,24] In our work, oil in water ME was used. The magnetic emulsion was obtained dispersing iron oxide in octane followed by dispersion in water using surfactants (ie, Sodium dodecyl sulfate). Therefore, magnetic emulsion has a significant percentage of nonmagnetic material on its composition (see TG measurements), which, in turn, contributes to decrease saturation magnetization to approximately 40.0 emu $g^{-1}$.

Both samples 2016 and 4016 showed superparamagnetic characteristics at room temperature. Furthermore, the saturation magnetization ($M_S$) for the samples 2016 and 4016 was approximately 35 emu $g^{-1}$ and 15.0 emu $g^{-1}$. In addition, for all samples, the $M_R/M_S$ ratio is found to be below 0.5 which is the expected value for randomly packed single domain particles, which is related to the superparamagnetic behavior.

The sample 4016 has the smallest value of $M_S$, which is associated to a high polymeric content. In core–shell nanoparticles, the percentage of nonmagnetic material was increased after coating the magnetic emulsion with PPDA. As a consequence, the $M_S$ values of core–shell particles decrease. This result is in agreement with the observed in TG measurements.

## 4.4 | Thermogravimetric analysis

Figure 3C,D shows the TG curves of ME seed, and samples 2016 and 4016, respectively. In the magnetic emulsion thermogram (Figure 3C), two main thermal degradation events could be observed: (a) at the temperature range from 25°C to 500°C, and (b) above 500°C. In the first event, an initial weight loss of approximately
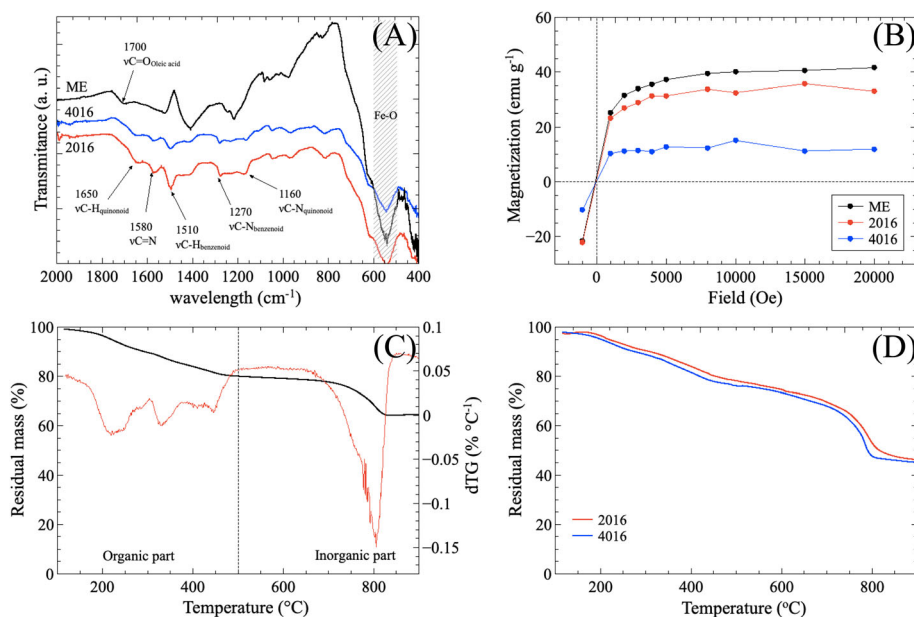


**FIGURE 3** Characterization of magnetic emulsion (ME) and samples 2016 and 4016: (A) Fourier transformed infrared (FTIR) spectra, (B) Magnetization curves, (C) thermogravimetric analysis (TG) and derivative TG (dTG) curves of ME seed, and (D) TG curves of samples 2016 and 4016 [Colour figure can be viewed at wileyonlinelibrary.com]

20% was observed. As indicated by dTG curve, at this temperature range, a large amount of organic matter (which consists of oleic acid surfactants) is expected to be degraded. When the temperature is between 500°C and 700°C, the second thermal degradation event, it was found an additional weight loss of 2.5%. This one is associated to the phase transition from $Fe_3O_4$ to $\gamma$-$Fe_2O_3$ + $\alpha$-$Fe_2O_3$. Above 700°C, $\gamma$-$Fe_2O_3$ is converted to FeO as demonstrated by Ayyappan, S and co-authors.[25]

The samples 2016 and 4016 exhibited the same degradation profile (Figure 3D). PVP degrades totally at ca. 600°C,[26] while PPDA starts to degrade at temperatures higher than 250°C.[21,27,28] In addition, the weight loss of sample 2016 was clearly less pronounced than sample 4016. Since the greater weight loss, the thicker is the polymer shell. This result indicates the sample 4016 has more polymer covering its surface than sample 2016.

## 4.5 | Particle size

Figure 4 shows the particle size distribution obtained for samples 2016 and 4016. According to the observed by TEM images, it was expected both samples exhibit almost the same size distribution. However, the sample 2016 exhibited a log-normal distribution with an average size of 319 nm, while sample 4016 shows a normal distribution with an average size of 395 nm.

Furthermore, the sample 2016 has a size distribution wider than the sample 4016 (Figure 4A,B, respectively). The widening of the size distribution may be associated with the particle agglomeration. After increasing the amount of PVP from 20 mg (sample 2016) to 40 mg (sample 4016) the narrowing in size distribution was observed. This result suggests that the PVP may act as steric barrier, avoiding the agglomeration of particles, even after the polymerization process.

## 4.6 | Electrodeposition studies

On the basis of the aforementioned results, the sample obtained with 40 mg of PVP and 16 mmol of PDA (sample 4016) was chosen as an ideal core–shell nanoparticle, with narrowed size distribution and superparamagnetic properties, to be applied in biosensors. Thus, to check the potential of a device containing our nanoparticles, a fully

integrated biosensor platform was used to perform electrodeposition studies. Such biosensor consists of four gold working electrodes (WEs), platinum counter electrode (CE), and Ag/AgCl reference electrode (RE) (Figure 5A).

Electrochemical deposition of sample 4016 was carried out by using cyclic voltammetry technique. The electrochemical deposition was made in two different ways: First, the biosensor platform was dropped in the MNPs solution vertically (Figure 5B, set-up-(i)). Here, we considered that the electrochemical deposition of MNPs was not sufficient as there were little MNPs on gold surface, as can be seen in Figure 5C.

In order to enhance the electrodeposition of sample 4016, the biosensor was placed horizontally and a droplet of 60 μL of samples was deposited onto its surface using the same optimized electrochemical conditions (set-up-(ii), Figure 5B). Here, the rate of the nanoparticles electrodeposition was higher than the previous experimental configuration (Figure 5D).

When the biosensor was vertically placed in the solution (set-up-(i)), the core–shell nanoparticles go through the solution to the WEs' surface. However, only the nanoparticles at the interface WE/solution were able to be electrodeposited. On the other hand, for the horizontal configuration (set-up-(ii)), the nanoparticles go to the surface by gravity and enhanced the electrodeposition.

The solution of sample 4016, containing HCl and $NaNO_2$, was left at 4°C for 24 hours, and the same experimental parameters for MNPs electrodeposition were used. Here, the aim was to verify if the maximum diazotation of amino groups could enhance the electrodeposition. This sample was called 4016-b. At these conditions, the core–shell nanoparticles agglomerated in the solution, being also electrodeposited onto the surface.

## 4.7 | CV and EIS results

Figure 6 shows the CV and EIS curves obtained for samples 4016 and 4016-b. CV was carried out to characterize gold WE surface before and after electrodeposition of MNPs. The best deposition was observed for sample 4016. However, when compared with bare gold, the redox of sample 4016 peaks were weaker. Finally, for sample 4016-b (left 24 hours in HCl and $NaNO_2$ at 4°C), the redox
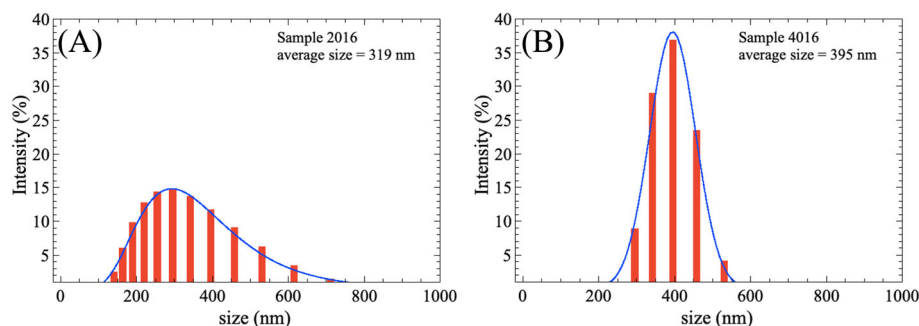


**FIGURE 4** Particle size distribution of (A) sample 2016 and (B) sample 4016 [Colour figure can be viewed at wileyonlinelibrary.com]
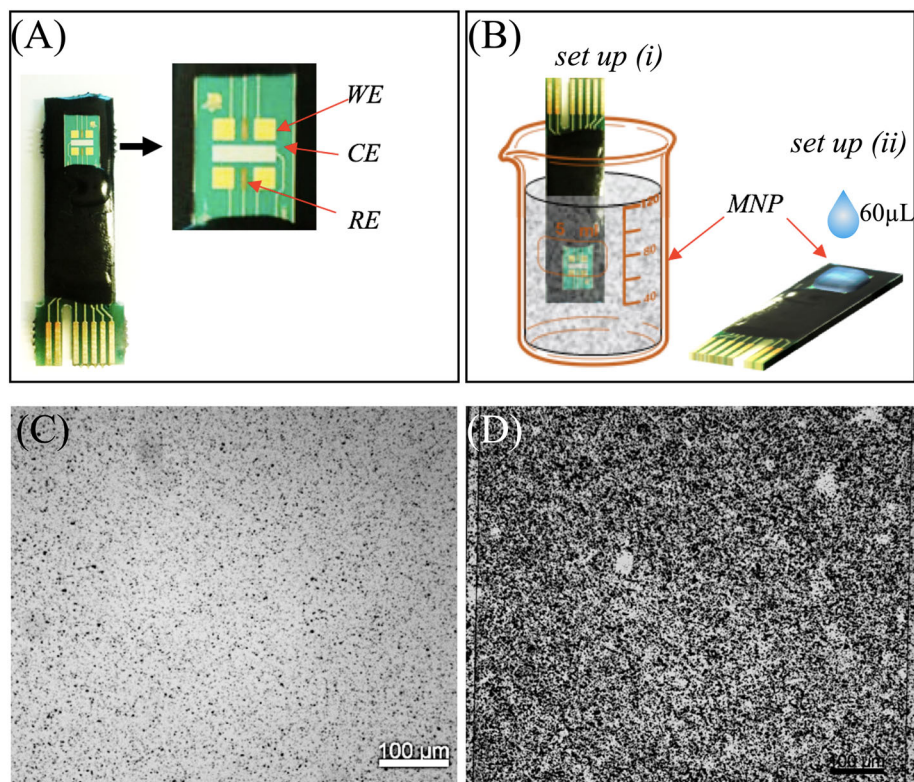
**FIGURE 5**　(A) Biosensor device with four working electrodes (WEs), counter electrode (CE), and reference electrode (RE). (B) Electrodeposition of MNP using (*i*) vertical position: the biosensor dropped in the MNP solution (*ii*) horizontal position: a droplet of 60 μL of MNP deposited onto gold WE surface. (C,D) Optical images of sample 4016 electrodeposited on gold WEs using the different experimental approach: (C) *set-up (i)*, and (D) *set-up (ii)* [Colour figure can be viewed at wileyonlinelibrary.com]

**FIGURE 6**　Curves of (A) cyclic voltammetry and (B) electrochemical impedance spectroscopy of samples 4016 and 4016-b. [Colour figure can be viewed at wileyonlinelibrary.com]
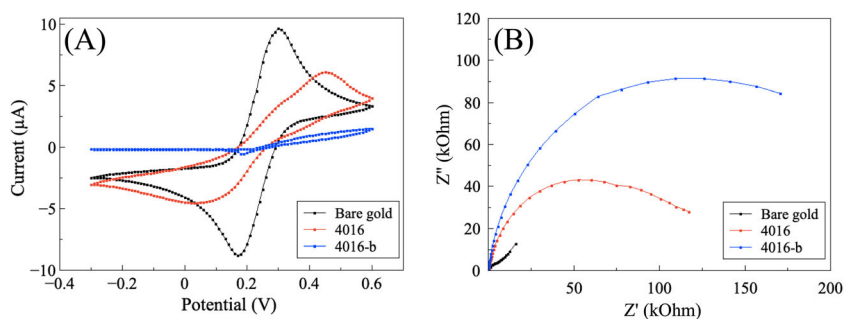


peaks have almost disappeared when compared with bare gold. This behavior is associated to nonhomogenous deposition of MNPs.

CV analyses were confirmed by EIS measurement. Comparing the bare gold with samples 4016 and 4016-b, the existence of a single semicircle indicates the presence of a single charge-transfer process, which was slightly affected by the presence of PPDA.[29] The sample 4016 has an increased impedance, which is in complete adequacy with CV because of the homogenous-deposited layer. The EIS has increased from 4016 to 4016-b. This is associated to an increase of charge resistance because of the increase of the passivation area onto gold WEs after electrochemical deposition of iron oxide–coated PPDA.

## 5 | CONCLUSIONS

In summary, we synthesized and characterized conducting magnetic particles based on PPDA, using magnetic emulsion as seed. Perfect core–shell nanoparticles, with narrowed size distribution and highly inorganic content, could be obtained when 40 mg of PVP and 0.16 mmol of *p*-phenylenediamine was used. After characterization, we found the core-shell nanoparticles have both superparamagnetic and electric properties with average size of 395 nm and magnetic saturation near 15 emu g$^{-1}$. The superparamagnetic property is very important to be used for fast separation, under magnetic field, when used for sample preparation, for instance. On the other hand, the

electric property may enhance the signal detection. In addition, because of the presence of $-NH_2$ groups in the polymer shell, covalent coupling of carboxylate-containing biomolecules (eg, oligonucleotides, proteins, and antibodies, specific ligands) can be easily performed. These very interesting characteristics make it possible our particles to be applied in sensors, *lab-on-a-chip*, microsystems, and microfluidics.

## ACKNOWLEDGEMENTS

## ORCID

*Ernandes Taveira Tenório-Neto* https://orcid.org/0000-0003-0257-3438

*Abdoullatif Baraket* https://orcid.org/0000-0002-1627-1353

*Marcos Rogério Guilherme* https://orcid.org/0000-0002-4260-5660

*Michele Karoline Lima-Tenório* https://orcid.org/0000-0003-3669-7025

*Abdelhamid Errachid* https://orcid.org/0000-0003-0092-2841

*Hatem Fessi* https://orcid.org/0000-0001-9223-0353

*Abdelhamid Elaissari* https://orcid.org/0000-0002-2151-9894

## REFERENCES

1. Chauhan M, Gaba A, Hong T, et al. Convenient and template-free route to one-pot green synthesis of polyrhodanine core-shell nanoparticles. *ACS Omega*. 2018;3(9):10974-10979. https://doi.org/10.1021/acsomega.8b01588

2. Srinivasan SY, Paknikar KM, Gajbhiye V, Bodas D. Magneto-conducting core/shell nanoparticles for biomedical applications. *Chemnanomat*. 2018;4(2):151-164. https://doi.org/10.1002/cnma.201700278

3. El Hassani NEA, Baraket A, Boudjaoui S, et al. Development and application of a novel electrochemical immunosensor for tetracycline screening in honey using a fully integrated electrochemical Bio-MEMS. *Biosens Bioelectron*. 2018. https://doi.org/10.1016/j.bios.2018.09.052;130:330-337.

4. Nawaz M, Sliman Y, Ercan I, et al. Magnetic and pH-responsive magnetic nanocarriers. In: *Stimuli Responsive Polymeric Nanocarriers for Drug Delivery Applications: Volume 2: Advanced Nanocarriers for Therapeutics*. Woodhead Publishing Series in Biomaterials. Elsevier Science; 2018:37-85https://books.google.com.br/books?id=KOZ0DwAAQBAJ.

5. Weber J, Thompson A, Wilmoth J, Batra VS, Janulaitis N, Kastner JR. Effect of metal oxide redox state in red mud catalysts on ketonization of fast pyrolysis oil derived oxygenates. *Appl Catal Environ*. 2019; 241:430-441. https://doi.org/10.1016/j.apcatb.2018.08.061

6. Xu H-Y, Li B, Shi T-N, Wang Y, Komarneni S. Nanoparticles of magnetite anchored onto few-layer graphene: a highly efficient Fenton-like nanocomposite catalyst. *J Colloid Interface Sci*. 2018;532:161-170. https://doi.org/10.1016/j.jcis.2018.07.128

7. Tenorio-Neto ET, Baraket A, Kabbaj D, et al. Submicron magnetic core conducting polypyrrole polymer shell: preparation and characterization. *Mater Sci Eng C-Materials Biol Appl*. 2016;61:688-694. https://doi.org/10.1016/j.msec.2015.12.052

8. Bhattacharjee Y, Chatterjee D, Bose S. Core–multishell heterostructure with excellent heat dissipation for electromagnetic interference shielding. *ACS Appl Mater Interfaces*. 2018;10(36):30762-30773. https://doi.org/10.1021/acsami.8b10819

9. Jamshaid T, Tenorio-Neto ET, Eissa MM, et al. Magnetic particles: from preparation to lab-on-a-chip, biosensors, microsystems and microfluidics applications. *TrAC - Trends Anal Chem*. 2016;79: 344-362. https://doi.org/10.1016/j.trac.2015.10.022

10. Reddy KR, Park W, Sin BC, Noh J, Lee Y. Synthesis of electrically conductive and superparamagnetic monodispersed iron oxide-conjugated polymer composite nanoparticles by in situ chemical oxidative polymerization. *J Colloid Interface Sci*. 2009;335(1):34-39. https://doi.org/10.1016/j.jcis.2009.02.068

11. Ma J, Li D, Zhong L, et al. Synthesis and characterization of biofunctional quaternized xylan-$Fe_2O_3$core/shell nanocomposites and modification with polylysine and folic acid. *Carbohydr Polym*. 2018; 199:382-389. https://doi.org/10.1016/j.carbpol.2018.07.003

12. Dzudzevic Cancar H, Soylemez S, Akpinar Y, et al. A novel acetylcholinesterase biosensor: core–shell magnetic nanoparticles incorporating a conjugated polymer for the detection of organophosphorus pesticides. *ACS Appl Mater Interfaces*. 2016;8(12):8058-8067. https://doi.org/10.1021/acsami.5b12383

13. Wang N, Li G, Yu Z, Zhang X, Qi X. Conductive polypyrrole/viscose fiber composites. *Carbohydr Polym*. 2015;127:332-339. https://doi.org/10.1016/j.carbpol.2015.03.076

14. Stejskal J. Polymers of phenylenediamines. *Prog Polym Sci*. 2015;41: 1-31. https://doi.org/10.1016/j.progpolymsci.2014.10.007

15. Targhoo A, Amiri A, Baghayeri M. Magnetic nanoparticles coated with poly(p-phenylenediamine-*co*-thiophene) as a sorbent for preconcentration of organophosphorus pesticides. *Microchim Acta*. 2017;185(1): 15. https://doi.org/10.1007/s00604-017-2560-1

16. Lakouraj MM, Zare EN, Moghadam PN. Synthesis of novel conductive poly(*p*-phenylenediamine)/$Fe_3O_4$ nanocomposite via emulsion polymerization and investigation of antioxidant activity. *Adv Polym Technol*. 2014;33(1). https://doi.org/10.1002/adv.21385

17. Jamshaid T, Tenorio-Neto ET, Eissa M, et al. Preparation and characterization of submicron hybrid magnetic latex particles. *Polym Adv Technol*. 2015;26(9):1102-1108. https://doi.org/10.1002/pat.3541

18. Goel A, Rani N. Effect of PVP, PVA and POLE surfactants on the size of iridium nanoparticles. *Open J Inorganic Chem*. 2012;02(03):67-73. https://doi.org/10.4236/ojic.2012.23010.

19. Montagne F, Mondain-Monval O, Pichot C, Elaissari A. Highly magnetic latexes from submicrometer oil in water ferrofluid emulsions. *J Polym Sci Part A-Polymer Chem*. 2006;44(8):2642-2656. https://doi.org/10.1002/pola.21391

20. Braconnot S, Eissa MM, Elaissari A. Morphology control of magnetic latex particles prepared from oil in water ferrofluid emulsion. *Colloid Polym Sci*. 2013;291(1):193-203. https://doi.org/10.1007/s00396-012-2700-4

21. Amer I, Mokrani T, Jewell L, Young DA, Vosloo HCM. Synthesis and characterization of sulfonated poly(*p*-phenylenediamine) prepared by different procedures. *Polymer*. 2015;66:230-239. https://doi.org/10.1016/j.polymer.2015.04.050

22. Baghayeri M, Zare EN, Lakouraj MM. A simple hydrogen peroxide biosensor based on a novel electro-magnetic poly(*p*-phenylenediamine)@$Fe_3O_4$ nanocomposite. *Biosens Bioelectron*. 2014; 55:259-265. https://doi.org/10.1016/j.bios.2013.12.033

23. Gao R, Mu X, Zhang J, Tang Y. Specific recognition of bovine serum albumin using superparamagnetic molecularly imprinted nanomaterials prepared by two-stagecore-shellsol-gel polymerization. *J Mater Chem B*. 2014;2(7):783-792. https://doi.org/10.1039/c3tb21424a

24. Eissa MM, Rahman MM, Zine N, et al. Reactive magnetic poly (divinylbenzene-*co*-glycidyl methacrylate) colloidal particles for specific antigen detection using microcontact printing technique. *Acta Biomater*. 2013;9(3):5573-5582. https://doi.org/10.1016/j.actbio.2012.10.027

25. Ayyappan S, Gnanaprakash G, Panneerselvam G, Antony MP, Philip J. Effect of surfactant monolayer on reduction of $Fe_3O_4$ nanoparticles under vacuum. *J Phys Chem C*. 2008;112(47):18376-18383. https://doi.org/10.1021/jp8052899

26. Peres-Filho MJ, Gaeti MPN, de Oliveira SR, Marreto RN, Lima EM. Thermoanalytical investigation of olanzapine compatibility with excipients used in solid oral dosage forms. *J Therm Anal Calorim*. 2011;104(1):255-260. https://doi.org/10.1007/s10973-010-1245-3

27. Liu F, Wang L, Yin Q, Jiang B. Optimization of thermoelectric figure of merit in poly(*p*-phenylenediamine)/exfoliated graphene nanosheets composites. *RSC Adv*. 2014;4(93):51558-51568. https://doi.org/10.1039/C4RA06249C

28. Amer I, Young DA. Chemically oxidative polymerization of aromatic diamines: the first use of aluminium-triflate as a co-catalyst. *Polymer*. 2013;54(2):505-512. https://doi.org/10.1016/j.polymer.2012.11.078

29. Manivel P, Sathiyanarayanan S, Venkatachari G. Synthesis of poly(*p*-phenylene diamine) and its corrosion inhibition effect on iron in 1MHC1. *J Appl Polym Sci*. 2008;110(5):2807-2814. https://doi.org/10.1002/app.28772

## SUPPORTING INFORMATION

Additional supporting information may be found online in the Supporting Information section at the end of the article.